COBEM 99
XV Congresso Brasileiro de Engenharia Mecânica
15th Brazilian Congress of Mechanical Engineering
22 - 26 de Novembro de 1999 / November 22 - 26, 1999 Águas de Lindóia, São Paulo,

FILLING OF RECTANGULAR MOLDS USING THE VOF METHOD AND A TVD DISCRETIZATION

Carlos E. Fontes
Paulo L. C. Lage
José C. Pinto
Programa de Engenharia Química, COPPE/UFRJ
CP 68502 – CEP 21945-970 – Rio de Janeiro, RJ, Brazil

Abstract. *Among the several issues that have to be faced for the simulation of the filling stage of a Reaction Injection Molding (RIM) process, the surface-tracking problem is one of the most challenging. In this paper, the equations of fluid motion have been discretized using a finite-volume method and the resulting system has been solved using the SIMPLER algorithm. The surface is captured using the Volume-of-Fluid method (VOF) which has been implemented using a high order upwind-TVD scheme that conserves the sharpness of interface. The numerical code has been tested against a benchmark solution for the backward facing step problem. Results for square-cavity filling for two systems (oil-water and air-water) have been obtained that show the capability of the numerical code to predict fluid entrapment and incomplete mold filling.*

Keywords*: Mold filling, TVD schemes, VOF schemes, computational fluid dynamics (CFD).*

1. INTRODUCTION

Reactive Injection Molding (RIM) is the process in which monomers are injected in a mold where chemical reaction will take place in order to product a plastic (polymer) that has the desired shape. Comparing to the injection of a polymer melt, this process needs much lower injection pressures during the mold filling stage. The polymerization systems that are adequate for such process are those with a very fast reaction rate. This large reaction rate provokes huge variations of bulk viscosity, temperature and composition, and moderate changes in density. Due to these severe conditions, the formation of more than one phase during the filling stage is also possible.

There exist several problems in achieving a good simulation of a RIM process, but in this paper only one is considered: the fluid dynamics prediction and surface tracking during the mold filling process. For this goal, computational fluid dynamics has been used to develop a numerical code that is capable of predicting the interface topology and the effects of fluid-fluid interfaces. Such code can be used as a mold design tool.

An important issue in the method of capturing a moving interface between two immiscible fluids is to work on the same Eulerian mesh used to solve the fluid flow equations for both fluids. Thus, the two fluids are modeled as a single continuum with property jumps at the interface. According to the volume-of-fluid (VOF) method, different values of a *color function* are used to mark the individual fluid particles. Therefore, the fluid-fluid interface is defined by the transitional region between these two values of the color function. The interface propagation is then obtained through the solution of a transient scalar advection equation in the Eulerian mesh. The numerical diffusion and oscillation problems, which are inherent to the solution of hyperbolic equations like the color function equation, have been addressed through the usage of a high order TVD-scheme. The conservation equations for mass and momentum have been solved by a finite-volume method using the SIMPLER algorithm, but surface tension effects at the interface were not included in the analysis. The fluid dynamics part of the code has been tested against a benchmark solution for the incompressible fluid flow over a backward-facing step. Then the code has been used to simulate the filling of a two-dimensional square mold, initially with oil or air, with water.

2. FLUID DYNAMICS EQUATIONS

The mass and momentum conservation equation for a pseudo-single-phase Newtonian fluid, with variable density and viscosity, are presented below in a dimensionless form.

$$\frac{\partial(\varphi)}{\partial\tau}+\mathrm{Re}_{ref}\cdot\frac{\partial(\varphi U)}{\partial X}+\mathrm{Re}_{ref}\cdot\frac{\partial(\varphi V)}{\partial Y}=0 \tag{1}$$

$$\frac{\partial(\varphi U)}{\partial\tau}+\mathrm{Re}_{ref}\cdot\frac{\partial(\varphi UU)}{\partial X}+\mathrm{Re}_{ref}\cdot\frac{\partial(\varphi VU)}{\partial Y}=-\mathrm{Re}_{ref}\cdot\frac{\partial P}{\partial X}-\left[\frac{\partial T_{xx}}{\partial X}+\frac{\partial T_{yx}}{\partial Y}\right] \tag{2}$$

$$\frac{\partial(\varphi V)}{\partial\tau}+\mathrm{Re}_{ref}\cdot\frac{\partial(\varphi UV)}{\partial X}+\mathrm{Re}_{ref}\cdot\frac{\partial(\varphi VV)}{\partial Y}=-\mathrm{Re}_{ref}\cdot\frac{\partial P}{\partial Y}-\left[\frac{\partial T_{xy}}{\partial X}+\frac{\partial T_{yy}}{\partial Y}\right] \tag{3}$$

$$T_{xx}=-2\Gamma\cdot\frac{\partial U}{\partial X}+\frac{2}{3}\cdot\Gamma\cdot\left[\frac{\partial U}{\partial X}+\frac{\partial V}{\partial Y}\right] \tag{4}$$

$$T_{yx}=T_{xy}=-\Gamma\cdot\left[\frac{\partial U}{\partial Y}+\frac{\partial V}{\partial X}\right] \tag{5}$$

$$T_{yy}=-2\cdot\Gamma\cdot\frac{\partial V}{\partial Y}+\frac{2}{3}\cdot\Gamma\cdot\left[\frac{\partial U}{\partial X}+\frac{\partial V}{\partial Y}\right] \tag{6}$$

where

$$X=\frac{x}{Din}\qquad Y=\frac{y}{Din}\qquad U=\frac{u}{vmed}\qquad V=\frac{v}{vmed} \tag{7}$$

$$P=\frac{p-\rho g_y y-\rho g_x x}{\rho\cdot vmed^2}\qquad \tau=\frac{\mu_{ref}\cdot t}{\rho_{ref}\cdot Din^2} \tag{8}$$

$$\mathrm{Re}_{ref} = \frac{Din \cdot vmed \cdot \rho_{ref}}{\mu_{ref}} \qquad \Gamma = \frac{\mu}{\mu_{ref}} \qquad \varphi = \frac{\rho}{\rho_{ref}} \tag{9}$$

and t is the time, x and y are the spatial coordinates, ρ is the density, μ is the viscosity, u is the velocity component in x direction, v is the velocity component in y direction, p is the pressure, g_i is the body force in i direction, Din is the inlet width and $vmed$ is the mean inlet velocity. ρ_{ref} e μ_{ref} refer to the inlet fluid properties (fluid 2).

After applying a finite-volume fully implicit discretization on a staggered grid using the power-law scheme, the solution has been achieved using the SIMPLER scheme (Patankar, 1980).

3. NUMERICAL MODEL VALIDATION

A backward facing step (BFS) benchmark (Gartling, 1990) has been used to verify the fluid-dynamics part of the developed code. The problem geometry is given in Fig. 1-a. In this simulation, the value of the Reynolds number (Re_{ref}), based on the inlet width (Din), was 400 (800 in the benchmark). All simulations that have been done had the inlet velocity given by a parabolic profile of the vertical velocity component, as can be seen in Eq. (10).

$$v(x) = A \cdot (B - x)(x - C) \tag{10}$$

valid for $B \leq x \leq C$. For the benchmark simulations, A =2400, B = 0.05 and C = 1.0, giving $vmed$ = 1. The pressure at outlet boundary was set to zero and the velocities continuity conditions were adopted at this position due to the large aspect ratio used ($LY = 30LX$). The non-slip condition has been used on all solid walls. Figure 1-b shows the flow field through the calculated streamlines. It is important to note that our results came from a dynamic simulation while the benchmark solution solves the steady-state equations. Figure 2 compares the results obtained for an 80×160 grid and those given by the benchmark solution at two Y positions. Good agreement is observed.

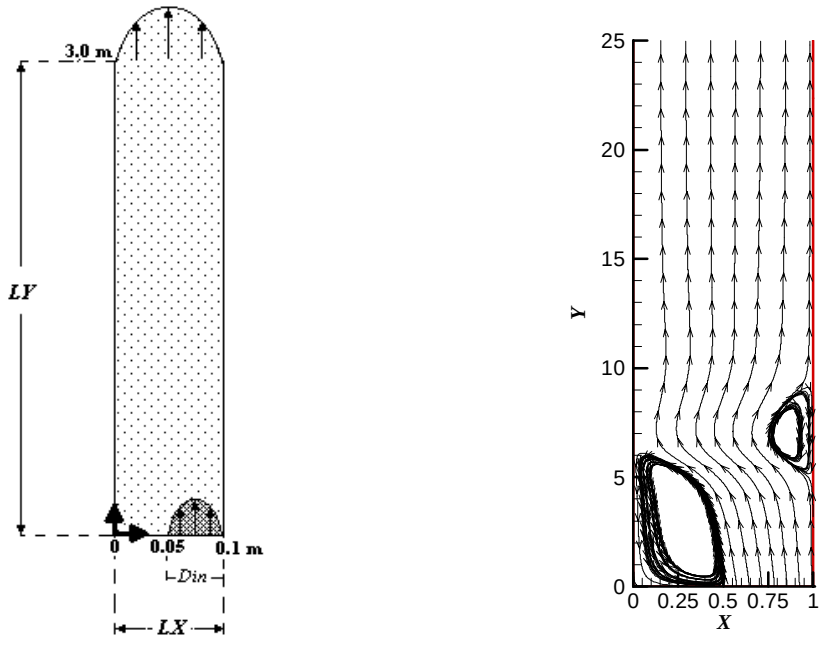

(a) (b)

Figure 1- Benchmark geometry (a) and streamlines of the calculated velocity field (b).

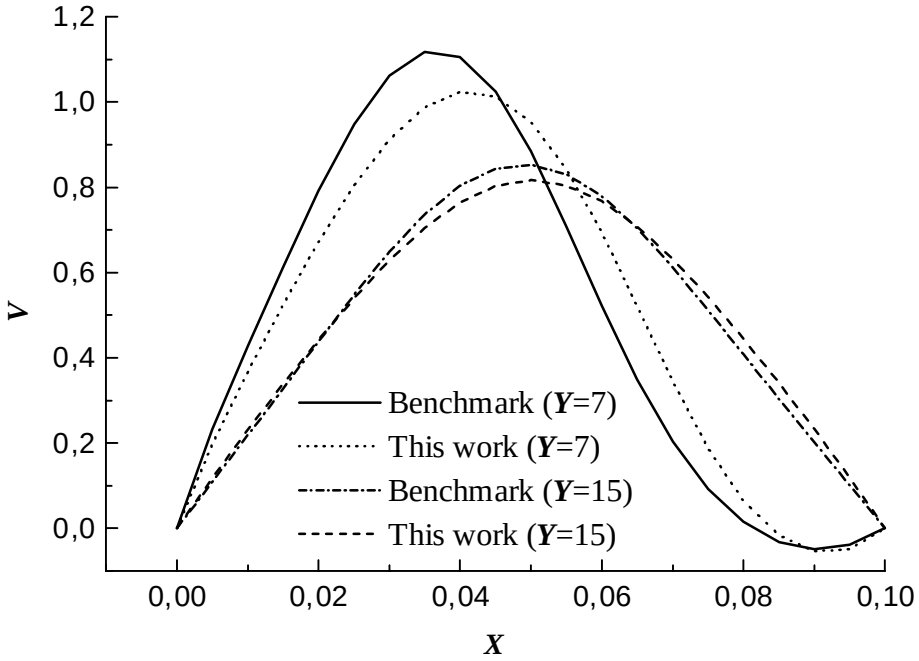

Figure 2- Comparison between benchmark and calculated results.

4. INTERFACE CAPTURING METHOD

Existing methods for the computation of free fluid-fluid interfaces can be classified into two groups (Ferziger & Pèric, 1997): surface fitting and surface capturing methods. For the methods in the first of these categories, the interface is represented and tracked explicitly either by marking it with special marker points, or by attaching it to a mesh surface which is forced to move with the interface. For the methods in the second category, the fluids on both sides of the interface are marked by either massless particles or an indicator (color) function.

The method used in this paper belongs to the second category, and was first used by Hirt & Nichols (1981). In the volume of fluid (VOF) method the advection of the color function *F*, given by Eq.(11), has to be solved. The *F* values are stored at in the staggered finite-volume grid similarly to pressure.

$$\frac{\partial F}{\partial \tau} + \mathrm{Re}_{ref} \cdot U \cdot \frac{\partial F}{\partial X} + \mathrm{Re}_{ref} \cdot V \cdot \frac{\partial F}{\partial Y} = 0 \tag{11}$$

For a given volume, *F* is equal to 0 when the volume has no inlet fluid (in other words, only fluid 1 is inside the mold), but it is equal to 1 when the volume is completely filled with the inlet fluid (fluid 2). The interface has *F*-values between 0 and 1. The dimensionless physical properties of the pseudo-single-phase fluid throughout the mold are given by

$$\varphi = (1 - F) \cdot \frac{\rho_1}{\rho_2} + F \tag{12}$$

$$\Gamma = (1 - F) \cdot \frac{\mu_1}{\mu_2} + F \tag{13}$$

Hirt and Nichols (1981) had solved Eq. (11) using a carefully limited donor-acceptor scheme. For each time step, this equation is solved explicitly and, in sequence, mass and momentum conservation equations are solved by the equation-by-equation iterative solution of SIMPLER. This methodology simplifies very much the capture of the interface, but numerical diffusion, which occurs due to the nature of Eq. (11), rule out the usage of first-order discretization methods. Higher-order methods decrease the effect of numerical diffusion but lead to numerical oscillations. Both are undesirable, because numerical diffusion spreads the interface destroying its sharpness, while numerical oscillations cause the accumulation or depletion of F in one cell far outside the defined [0,1] range. Several methods have been developed in order to solve the scalar advection problem with little numerical diffusion or oscillations. One of the most successful classes of methods was that based on Total Variation Diminishing (TVD) schemes.

5. TOTAL VARIATION DIMINISHING SCHEMES

A good summary of TVD schemes is given by Sweby (1984). It was Harten (1983) who has introduced and named such methods. Hannapel (1994) describes a numerical method as TVD if Eq.(14) is valid for scalar conservation laws. ξ is the transported variable and its total variation is defined in Eq. (15).

$$TV(\xi^{n+1}) \le TV(\xi^{n}) \tag{14}$$

$$TV(\xi) = \sum_{i} \left| \xi_i - \xi_{i-1} \right| \tag{15}$$

Chakravarthy & Osher (1985) described one-dimensional second- and third-order accurate TVD schemes with low truncation error. These schemes were used to solve advective equations, like Eq.(11), and systems of conservation laws (Euler equations). The construction of multidimensional algorithms is straightforward through the application of one-dimensional method coordinate-by-coordinate. However, Goodman and LeVeque (1985) have proved that there is no multidimensional TVD scheme, but Chakravarthy & Osher (1985) have shown that numerical results are extremely good. Chen et al. (1996) has applied this scheme to a two-dimensional spray atomization problem, obtaining good results too. Based on its simplicity and good results the Chakravarthy & Osher (1985) third-order scheme has been used in the present work.

The explicit discretized form of Eq.(11) is given by Eq.(16). The F-fluxes at the faces of the volumes are determined using the upwind-TVD scheme. For example, for east face, the flux is given by Eqs. (17) to (26). In these equations the index P means position (i, j), E position $(i+1, j)$, e position $(i+1/2, j)$, ee position $(i+3/2, j)$, w position $(i-1/2, j)$, n position $(i, j+1/2)$, s position $(i, j-1/2)$. When γ equals 1/3 and β equals 4 these equations correspond to a third-order upwind scheme. Equation (18) represents the flux given for the Engquist-Osher first-order scheme for the present flux function (Osher & Chakravarthy, 1984). The minmod function is defined by Eq. (24) and used to define the limited fluxes given in Eqs. (20)-(23). The flux limitation is responsible for avoiding numerical oscillations in the solution. The fluxes for the other faces are obtained by obvious changes of subscripts.

$$F_P = F_P^o - \mathrm{Re}_{ref}\, \delta\tau \left[\frac{U_P \cdot (F_e - F_w)}{\delta X} + \frac{V_P \cdot (F_n - F_s)}{\delta Y} \right] \tag{16}$$

$$U_P F_e = U_k F_{k+\frac{1}{2}} = f_e + h_e \tag{17}$$

$$f_e = f_{k+\frac{1}{2}} = \max[0, U_k] F_k - \max[0, -U_k] F_{k+1} \tag{18}$$

$$h_e = \frac{1}{4}\left[\left(\overline{d\phi}_e^{+} + \overline{\overline{d\phi}}_w^{+}\right) + \gamma\left(\overline{d\phi}_e^{+} - \overline{\overline{d\phi}}_w^{+}\right)\right] - \frac{1}{4}\left[\left(\overline{\overline{d\phi}}_e^{-} + \overline{d\phi}_{ee}^{-}\right) + \gamma\left(\overline{\overline{d\phi}}_e^{-} - \overline{d\phi}_{ee}^{-}\right)\right] \tag{19}$$

$$\overline{d\phi}_e^{+} = \text{minmod}(d\phi_e^{+}, \beta d\phi_w^{+}) \tag{20}$$

$$\overline{\overline{d\phi}}_w^{+} = \text{minmod}(d\phi_w^{+}, \beta d\phi_e^{+}) \tag{21}$$

$$\overline{\overline{d\phi}}_e^{-} = \text{minmod}(d\phi_e^{-}, \beta d\phi_{ee}^{-}) \tag{22}$$

$$\overline{d\phi}_{ee}^{-} = \text{minmod}(d\phi_{ee}^{-}, \beta d\phi_e^{-}) \tag{23}$$

$$\text{minmod}(a,b) = \text{sign}(a) \cdot \max\{0, \min[|a|, b\,\text{sign}(a)]\} \tag{24}$$

$$d\phi_e^{+} = d\phi_{k+\frac{1}{2}}^{+} = U_k \cdot (F_{k+1} - F_k) \qquad , \mathrm{U_k} > 0 \tag{25}$$

$$d\phi_e^{-} = d\phi_{k+\frac{1}{2}}^{-} = U_k \cdot (F_{k+1} - F_k) \qquad , \mathrm{U_k} \le 0 \tag{26}$$

Boundary conditions for this equation are obvious: every cell before inlet volumes is considered to be full of fluid 2 (F = 1), and all cells after the outlet are considered to be full of fluid 1 (F = 0). In the beginning of the filling process, the mold is filled with fluid 1 (F = 0).

In this section, all the equations refers to a discretization of Eq. (11) in its non-conservative form. This is due to the characteristics of Osher & Chakravarthy TVD scheme which shows large error accumulation if one uses the conservative form.

6. SIMULATION RESULTS

All the simulations presented in the following have been obtained for the filling of a square mold with one inlet and one outlet, as shown in Fig. 3 ($LX = LY$). In this figure, Din and Dout are, respectively, the inlet and outlet lengths. They both equals 25 mm. Dimensions LXD and LYD equals 0.1 m. The inlet parabolic v profile is given by Eq. (10) with A =240, B = 0.05 and C = 1.0, which corresponds to a average inlet velocity of 0.1 m/s. The outlet velocity field is easily determined from the mold geometry, global mass conservation and Eq. (10). The velocities at all other walls are zero (non-slip condition). The mold is considered to be full of a fluid 1 that is displaced by fluid 2. Fluid 2 is water, but fluid 1 is oil or air, depending upon the case. Initially, the fluid inside the mold is at rest. The physical properties of the fluids are summarized in Table 1. For the air-water simulation, a convergence problem has appeared in the fluid-flow solution algorithm, which is caused by the large density difference between the two fluids (three orders of magnitude). The SIMPLER algorithm has

been developed for moderate changes of the fluid density, and the present implementation is able to simulate mold filling with ρ_2/ρ_1 only up to 100.

Simulations using different ratios between fluid densities (up to 100) have shown that the flow behavior of the outlet fluid is somewhat affected as the density ratio changes. However, these same simulations have shown that the density ratio effect on the flow results for the inlet fluid is very small which has allowed the prediction of the filling behavior using a different density ratio when this was necessary to avoid numerical difficulties. Thus, for the air-water case, the densities of both fluids have been considered equal. For all simulations, a 56×56 grid has been used, because simulations using finer grids have shown that this grid gives fair accurate results.

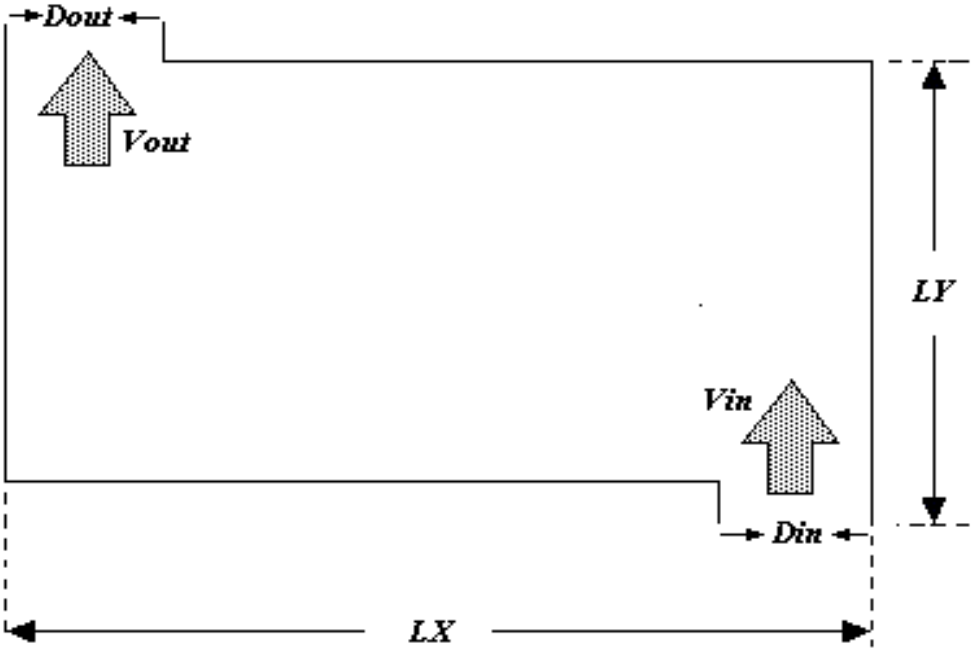

Figure 3- Two-dimensional rectangular mold.

Table 1- Physical properties of the fluids.

Fluid	ρ (kg/m^3)	μ (Pa.s)
Water	1.0×10^3	1.0×10^{-3}
Oil	885	0.486
Air	1.2	1.8×10^{-5}

Figures 4 and 5 shows the velocity and pressure fields after 2 s of filling for the two systems studied under Re_{ref} = 2500. In Fig. 4, however, it is possible to verify that the growing vortices are much more developed in Fig. 5. It is thus clear that the system air-water develops these fields much quicker than the oil-water system. These results were expected because the oil viscosity is much larger than air viscosity.

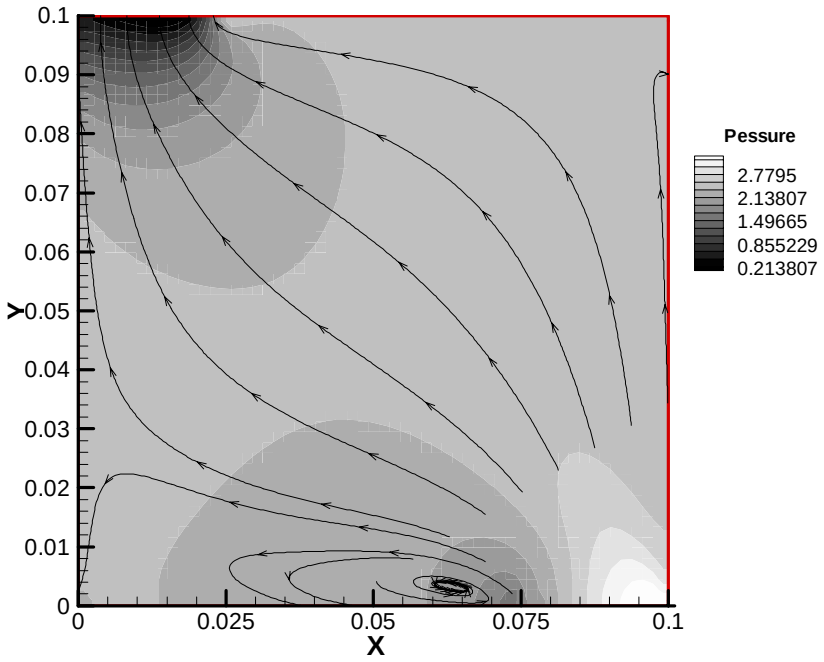

Figure 4- Velocity and pressure fields for oil-water simulation (Re_{ref} = 2500, t = 2 s).

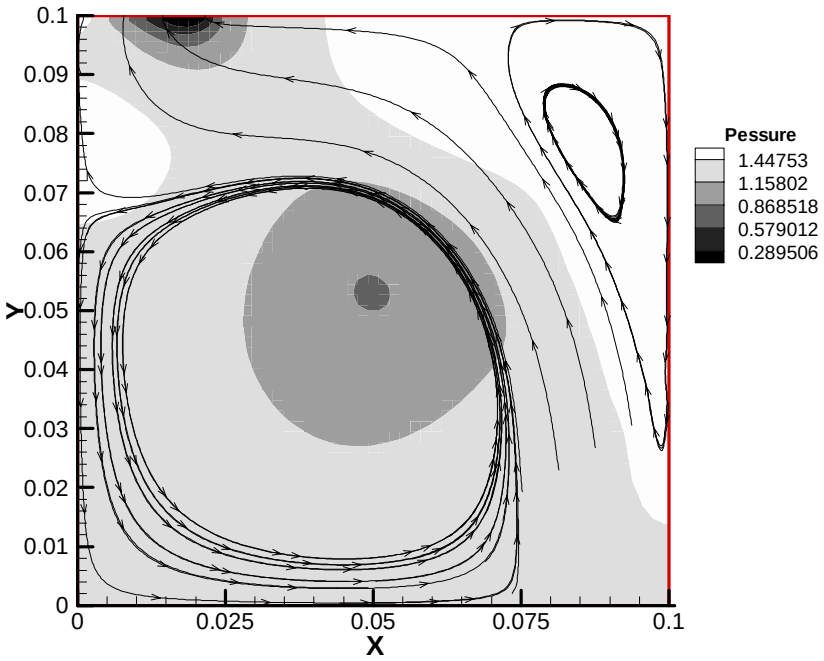

Figure 5- Velocity and pressure fields for air-water simulation (Re_{ref} = 2500, t = 2 s).

Figures 6 and 7 show the interface topology after 2 s. From these figures, it is clear that water has great difficult to enter the mold filled with oil, but moves almost freely through the mold that contains only air.

Figure 8 shows the interface position for the water-air system after 3,5 s of filling. The same filling pattern is observed for the oil-water system after 10s. Due to the vortices formed near the top-right and bottom-left corners of the mold, it becomes impossible to fill the chosen mold. This geometry has been chosen on purpose to show that the developed code can be used as a mold-designing tool.

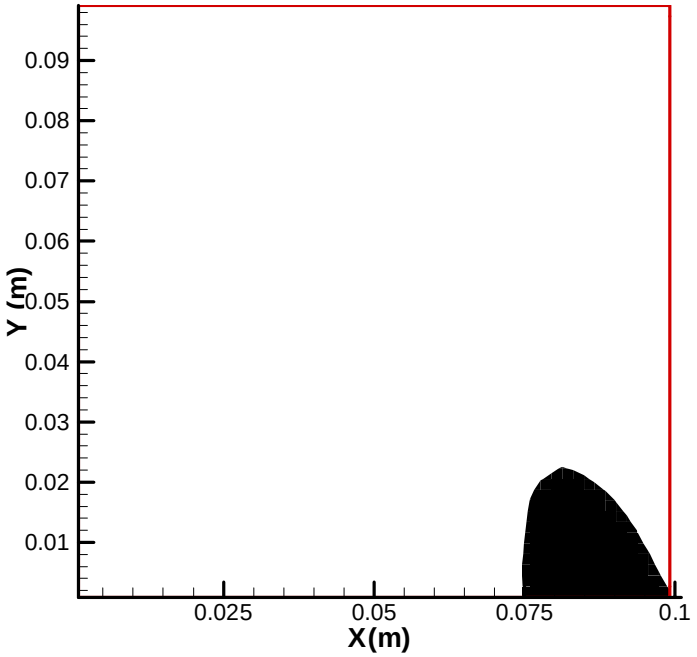

Figure 6- Interface position for the oil-water system (Re_{ref} = 2500, t = 2 s).

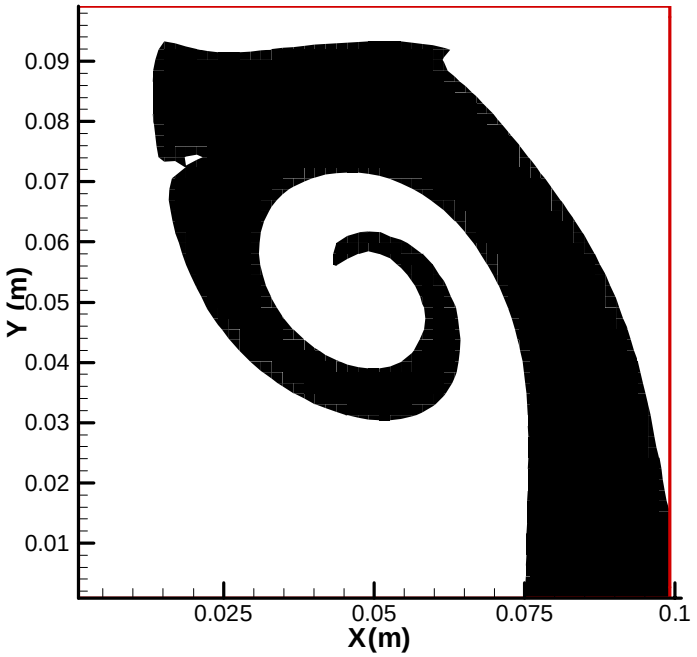

Figure 7- Interface position for the air-water system (Re_{ref} = 2500, t = 2 s).

6. CONCLUSIONS

This work develops a numerical code capable of simulating the mold filling process of rectangular two-dimensional cavities. The fluid dynamics part of the code was tested against a benchmark solution for a backward-facing step, with good agreement. Simulations of the mold filling process have been accomplished for oil-water and air-water systems. A limitation of the code for very large density ratio is verified and avoided in the air-water simulations. The results have shown that this code can be used as a tool for mold design.

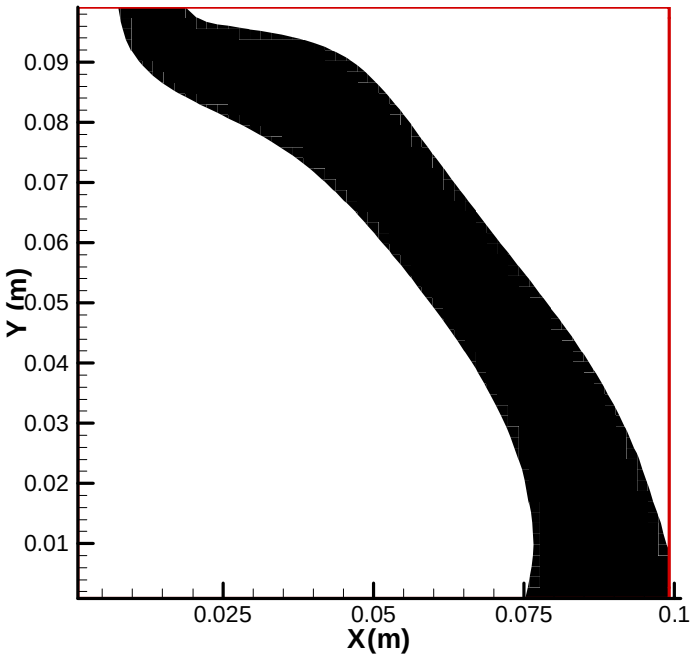

Figure 8- Interface position for the air-water system (Re_{ref} = 2500, t = 3.5 s).

ACKNOWLEDGEMENTS

The authors acknowledge the financial support obtained from CAPES and from CNPq, grant number 520660/98-6. This work has also been partially supported by NACAD/COPPE through the allocation of supercomputer resources.

REFERENCES

Chakravarthy, S.R. & Osher,S., 1985, A New Class of High Accuracy TVD Schemes for Hyperbolic Conservation Laws, AIAA paper 85-0363

Chen, Y-S et al., 1996, Combined Eulerian-Lagragian Method for General Gas-Liquid Flow Applications, Numerical Heat Transfer, Part B, vol.30, pp 409-422.

Ferziger, J.H & Peric, M., 1997, Computational Methods for Fluid Dynamics, Springer, New York

Gartling, D.K., 1990, A Test Problem for Outflow Boundary Conditions - Flow over a Backward Facing Step, International Journal for Numerical Methods in Fluids, vol.11, pp 953-967.

Goodman, J.B. & LeVeque, R.J., 1985, On the Accuracy of Stable Schemes for 2-D scalar Conservation Laws, Math. Comp., vol. 45, p.15

Harten, A., 1983, High Resolution Schemes for Hyperbolic Conservation Laws, Journal of Computational Physics, vol 135, pp. 260-278.

Hannapel, R., 1995, A Comparison of ENO and TVD Schemes for the Computation of Shock-Turbulence Interaction, Journal of Computational Physics, vol. 121, pp. 176-184.

Osher, S., & Chakravarthy, S., 1984, Very High Order Accurate TVD Schemes, ICASE Report no. 84-44, ICASE – NASA Langley Research Center, Hampton, Virginia.

Patankar, S.V., 1980, Numerical Heat Transfer and Fluid Flow, McGraw-Hill, New York.

Sweby, P.K., 1984, High Resolution Schemes Using flux Limiters for Hyperbolic Conservation Laws, SIAM Journal of Numerical Analysis, vol.21, n.5, pp. 995-1011